

# Study of Microstructural Characterization and Ionic Conductivity of a Chemical-Covalent Polyether–Siloxane Hybrid Doped with LiClO<sub>4</sub>

Wuu-Jyh Liang,<sup>†</sup> Ying-Pin Chen,<sup>‡</sup> Chien-Pang Wu,<sup>‡</sup> and Ping-Lin Kuo<sup>\*‡</sup>

Fire Protection and Safety Research Center and Department of Chemical Engineering,  
National Cheng Kung University, Tainan, Taiwan 70101, Republic of China

Received: March 1, 2005; In Final Form: October 26, 2005

The chemical-covalent polyether–siloxane hybrids (EDS) doped with various amounts of LiClO<sub>4</sub> salt were characterized by FT-IR, DSC, TGA, and solid-state NMR spectra as well as impedance measurements. These observations indicate that different types of complexes by the interactions of Li<sup>+</sup> and ClO<sub>4</sub><sup>−</sup> ions are formed within the hybrid host, and the formation of transient cross-links between Li<sup>+</sup> ions and ether oxygens results in the increase in  $T_g$  of polyether segments and the decrease in thermal stability of hybrid electrolyte. Initially a cation complexation dominated by the oxirane-cleaved cross-link site and PEO block is present, and after the salt-doped level of O/Li<sup>+</sup> = 20, the complexation through the PPO block becomes more prominent. Moreover, a significant degree of ionic association is examined in the polymer–salt complexes at higher salt uptakes. A VTF-like temperature dependence of ionic conductivity is observed in all of the investigated salt concentrations, implying that the diffusion of charge carrier is assisted by the segmental motions of the polymer chains. The behavior of ion transport in these hybrid electrolytes is further correlated with the interactions between ions and polymer host.

## Introduction

Polymer electrolytes are polymer-based systems that show ionic conductivity, which allows their use in solid-state devices such as batteries and capacitors.<sup>1–4</sup> Among the first and most studied host for polymer electrolytes is poly(ethylene oxide) (PEO), which is a polymer that dissolves high concentrations of a wide variety of salts to form polymeric electrolytes.<sup>5</sup> This conventional ion-conducting polymer has, in general, a multiphase nature consisting of a salt-rich crystalline phase with conductivity appreciable only above 65 °C,<sup>6</sup> a pure PEO spherulite crystalline phase, and an amorphous phase with dissolved salt. Ionic conduction generally used to be considered a property of the amorphous phase and, in addition, ionic association, ion–polymer interactions, and local relaxations of the polymer strongly influence ionic mobility.<sup>3,7–9</sup> Consequently, with the aim of enhancing ionic conductivity, efforts have been made to obtain polymer hosts with reduced crystallinity, high solvating power, and low glass transition temperature.

In recent years, considerable advance has been gained by designing new polymer electrolytes based on organic–inorganic hybrids or nanocomposite systems among which silica-based materials hold a prominent place. A variety of organic–inorganic hybrids presenting covalent bonds or only weak physical bonds (hydrogen bonding or van der Waals bonds) between the inorganic (siloxane) and organic (polymer) phases have been proposed.<sup>10–17</sup> These solid polymer electrolytes, so-called ormolytes, combine the solvating power of the ether units with the presence of an inorganic network, which provides higher chemical stabilities and better mechanical properties than

pure organic polymers.<sup>18,19</sup> The hybrid concept seems to be particularly well-adapted for the production of advanced solid materials presenting ion-conducting properties, with the advantage of replacing viscous liquid systems by solid or rubbery materials.<sup>20,21</sup>

In an effort to design a new class of organic–inorganic hybrid electrolyte consisting of a completely amorphous phase, and possessing excellent mechanical and chemical properties, in our previous study,<sup>22</sup> the chemical-covalent polyether–siloxane hybrids were prepared on the basis of poly(ethylene glycol) diglycidyl ether (PEGDE) blended with 3-glycidoxypolytrimethoxysilane (GPTMS) in various ratios, using  $\alpha,\omega$ -diaminopoly(propylene oxide) (Jeffamine D2000) as the curing agent. All of the resulting hybrids have good chemical stability in the liquid electrolyte (1M LiClO<sub>4</sub>/PC). With a 75 wt % liquid electrolyte solution, the plasticized hybrid electrolyte with the weight ratio of PEGDE/GPTMS = 2.0 exhibits an ionic conductivity of  $5.3 \times 10^{-3}$  S cm<sup>−1</sup> at 95 °C and  $1.4 \times 10^{-3}$  S cm<sup>−1</sup> at 15 °C, and also the film possesses good apparent mechanical property. The use of this promising material motivates the study of ionic dissociation and transport phenomena in polymer host/salt binary systems. The ion–polymer and ion–ion interactions are examined by FT-IR spectroscopy, DSC, and solid-state <sup>13</sup>C and <sup>7</sup>Li MAS NMR techniques. These results are correlated with ionic conductivity studies performed with use of impedance spectroscopy. Thermogravimetric analysis (TGA) is used to characterize thermal stability.

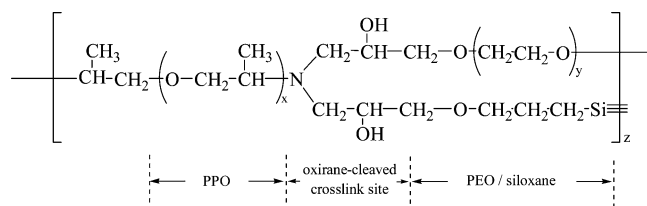
## Experimental Section

**Materials.** Poly(ethylene glycol) diglycidyl ether (PEGDE, Kyoeisha Chemical Co., Ltd.) and  $\alpha,\omega$ -diaminopoly(propylene oxide) (Jeffamine D2000, Huntsman Corporation) were dehydrated at 80 °C under vacuum for 24 h prior to use. 3-Glycidoxypolytrimethoxysilane (GPTMS, Dow Corning Corpora-

\* To whom all correspondence should be addressed. Phone: +886-6-275 7575, ext. 62658. Fax: +886-6-276 2331. E-mail: plkuo@mail.ncku.edu.tw.

<sup>†</sup> Fire Protection and Safety Research Center.

<sup>‡</sup> Department of Chemical Engineering.

**CHART 1: Schematic Structure of the Polyether–Siloxane Hybrid, EDS**


tion), lithium perchlorate ( $\text{LiClO}_4$ , Aldrich), and tetrahydrofuran (THF, Tedia) were used as received. All solvents were reagent grade or were purified by standard methods.

**Sample Preparation.** The organic–inorganic hybrids of polyether–siloxane– $\text{LiClO}_4$  were obtained via the sol–gel approach. First, the desired amounts of GPTMS were dissolved in an appropriate amount of THF and then hydrolyzed under acidic condition with HCl as the catalyst. The molar ratio between the reagents was  $\text{H}^+/\text{H}_2\text{O}/\text{Si} = 0.04/3/1$ . The volume ratio GPTMS:THF = 45:55 was used. Subsequently, a mixture of PEGDE (the weight ratio of PEGDE/GPTMS = 2.0) and the stoichiometric amount of D2000 as well as the desired amounts of lithium perchlorate were added under vigorous stirring. These solutions were then poured into an aluminum plate, and followed by slowly removing the solvent at room temperature, then cured at 100 °C for 24 h and 155 °C for 2 h. The thickness of the resulting films was controlled to be in the range of 150–200  $\mu\text{m}$ . These specimens were dried under vacuum at 80 °C for 72 h and then stored in an argon-filled glovebox (Vacuum Atmosphere Company, USA) for cell assembly. The undoped hybrid film (EDS) was also made in the same way without adding  $\text{LiClO}_4$ . Samples are labeled as EDS- $x$ , where  $x$  refers to the molar ratio of ether oxygen to lithium perchlorate ( $\text{O}/\text{Li}^+$ ). All of the resulting hybrid films were flexible, transparent, and brownish. The schematic structure for the polyether–siloxane hybrid is shown in Chart 1.

**Characterizations.** *FT-IR.* FT-IR spectra were measured by using a Nicolet 550 system with a wavenumber resolution of 2  $\text{cm}^{-1}$ , and a minimum of 64 scans were signal-averaged at room temperature under dry air atmosphere. Each sample was prepared by mixing with potassium bromide (KBr) pellet, and films were vacuum dried at 80 °C for several days to remove the absorbed water in the sample.

*Solid-State NMR.* High-resolution solid-state NMR experiments were carried out on a Bruker AVANCE 400 spectrometer, equipped with a 7 mm double-resonance probe. The Larmor frequencies for  $^1\text{H}$ ,  $^7\text{Li}$ , and  $^{13}\text{C}$  nuclei are respectively 400.17, 155.45, and 100.58 MHz. Magic angle spinning (MAS) of the samples in the range of 3–5 kHz was employed for obtaining NMR spectra. The Hartmann–Hahn condition for  $^1\text{H} \rightarrow ^{13}\text{C}$  cross-polarization (CP) experiments was determined with use of adamantane. The  $\pi/2$  pulse lengths for  $^1\text{H}$  and  $^7\text{Li}$  were typically 4 and 6  $\mu\text{s}$ , respectively. Typically, a repetition time of 5 s was used in all the NMR experiments. The  $^{13}\text{C}$  and  $^1\text{H}$  chemical shifts were externally referenced to tetramethylsilane (TMS) at 0.0 ppm.  $^7\text{Li}$  chemical shifts were referenced to solid  $\text{LiCl}$ .

*DSC.* Differential scanning calorimeter (DSC) (Du Pont TA2010) measurements were conducted over the temperature ranges of –150 to 200 °C at a heating rate of 10 °C/min under dry nitrogen atmosphere. In the first scan, a heating rate of 10 °C/min was used over the temperature range –150 to +200 °C. The second scan was performed after annealing the same sample used in the first scan at 200 °C for 10 min to remove

any prior thermal history, and then the sample was quenched and the same procedure repeated as for first scan. Glass transition temperature ( $T_g$ ) was reported as the midpoint of the transition process. All the thermograms are baseline corrected and calibrated against indium metal. An empty aluminum pan was used as a reference.

*TGA.* TGA analyses were carried out with a thermogravimetric analyzer (Perkin-Elmer TGA 7) over a temperature range of 100–800 °C at a heating rate of 20 °C/min under nitrogen atmosphere.

*Ionic Conductivity Measurements.* Alternating current impedance measurements of the samples were performed with a CH Instrument Model 604A Electrochemical Analyzer (CH Instruments, Inc., USA) under an oscillation potential of 10 mV from 100 kHz to 10 Hz. All the thin electrolyte films were sandwiched by two polished stainless steel blocking electrodes for conductivity tests. The presented ionic conductivity values ( $\sigma$ ) are obtained from the relationship  $\sigma = t/(R_b A)$ , where  $R_b$  is the bulk electrolyte resistance,  $t$  is the thickness, and  $A$  is the area of the sample.

**Results and Discussion**

**FT-IR Studies.** FT-IR spectroscopy was employed to study the interaction behavior between the ion and the hybrid host. Figure 1 shows the FT-IR spectra for the salt-free EDS and EDS/ $\text{LiClO}_4$  systems. As evidenced in this figure, it is obvious that when the concentration of  $\text{LiClO}_4$  salt increases in the hybrid complexes, the frequencies and intensities of the stronger bands change significantly, indicating that the introduction of salt into the hybrid network can change the intermolecular interactions, and the band at around 625  $\text{cm}^{-1}$  assigned to the  $\nu_4$  mode of the  $\text{ClO}_4^-$  anion<sup>23</sup> is broadened and split. These observations indicate that with the increase of  $\text{LiClO}_4$  uptake, three distinct phenomena could take place in the electrolytic complexes: (a) the gradual modification of the hydrogen-bonding structure, (b) the step by step modulation of the conformation of polyether chains, and (c) the manifestation of ionic pairing or ionic association.

Figure 1a shows the hydroxyl-stretching region of the FT-IR spectra for the salt-free EDS and EDS/ $\text{LiClO}_4$  systems. Obviously, a slightly progressive shift in the maximum of the hydroxyl stretching band to lower wavenumber with increasing  $\text{LiClO}_4$  concentration is observed. In addition, a further hydroxyl stretching vibration is detected around 3250  $\text{cm}^{-1}$  for each hybrid complex, which is ascribed to the –OH stretching vibration of the hydroxyls hydrogen bonded to perchlorate ions ( $\text{ClO}_4^-$ ).<sup>24</sup> Changes in FT-IR can be ascribed to the interactions between hydroxy groups and ions. Since an ion–dipole interaction is stronger than a dipole–dipole interaction, a negative shift in the wavenumber takes place.

Figure 1b shows that as the concentration of  $\text{LiClO}_4$  salt increases, the significant changes are detected in the band intensities ascribed to the C–O–C and the vibration mode of  $\nu_4(\text{ClO}_4^-)$ . Changes in the intensity, shape, and position of the C–O–C stretching mode are associated with the polyether– $\text{LiClO}_4$  interactions, whereas the  $\nu_4(\text{ClO}_4^-)$  stretch reflects the ion–ion interactions in these electrolytes. In the 1200–1000  $\text{cm}^{-1}$  region, the changes in –C–O– vibrations with increasing  $\text{LiClO}_4$  uptake can be attributed to the oxygen ligands of polyether chains interacting with acceptor groups to a greater extent in these hybrids, and are correlated to the lithium cation coordination. It was proposed that the electron shift toward the oxygen atom in the –C–O bond is associated with a decrease in the frequency and an increase in the intensity of the –C–O

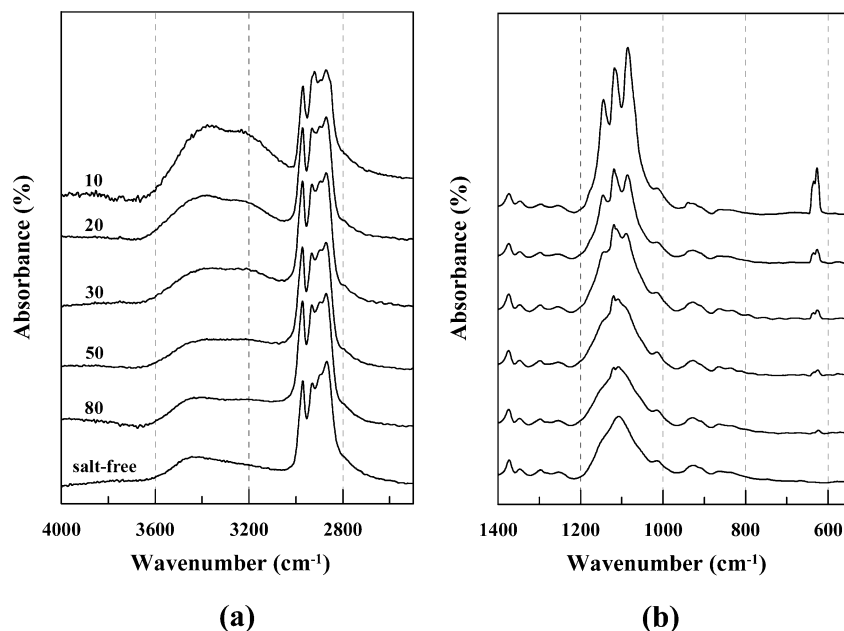


**Figure 1.** FT-IR spectra recorded of EDS–LiClO<sub>4</sub> electrolytes with various LiClO<sub>4</sub> uptakes (O/Li<sup>+</sup>) in the frequency range from (a) 4000 to 2500 cm<sup>−1</sup> and (b) 1400 to 500 cm<sup>−1</sup>.

stretching vibration with respect to those observed in the “free” ligands.<sup>25,26</sup> As the concentration of LiClO<sub>4</sub> salt increases in the hybrid complexes, two phenomena take place: (a) the concentration of oxygen atoms in polyether chains that are coordinated with Li<sup>+</sup> ions increases, thereby giving rise to a decrease in frequency and an increase in intensity of the –C–O stretching band, and (b) the concentration of hydrogen-bonded structures decreases, giving rise to an increase in frequency and a decrease in intensity of the involved band.

To study the ion–ion interactions, the spectral features of the  $\nu_4(\text{ClO}_4^-)$  mode appearing at around 625 cm<sup>−1</sup> were fitted with a Gaussian–Lorentzian function using Grams 386 deconvolution software (Galatic). As a result of the deconvolution, the lower and higher frequency components appeared at around 624 and 633 cm<sup>−1</sup>, respectively. Salomon et al.<sup>27</sup> suggest that the  $\nu_4(\text{ClO}_4^-)$  band centered at ~623 cm<sup>−1</sup> can be attributed to spectroscopically free ClO<sub>4</sub><sup>−</sup> anions, whereas the band centered at ~635 cm<sup>−1</sup> is associated with the presence of contact-ion pairs. The fraction of “free” anions can be calculated as the ratio of the area under the ~623 cm<sup>−1</sup> mode to the total area under the  $\nu_4(\text{ClO}_4^-)$  envelope. As can be seen in Figure 2, for the sample doped with the LiClO<sub>4</sub> content of O/Li<sup>+</sup> = 80, one concludes that the majority of the ClO<sub>4</sub><sup>−</sup> anions exist as spectroscopically “free” species; meanwhile, the Li<sup>+</sup> cations accept the electrons from the oxirane-cleaved cross-link site of polymer host and ether oxygens of the hybrid network in an “acceptor–donor” configuration (see <sup>7</sup>Li MAS NMR). With further addition of LiClO<sub>4</sub> salt, more and more free ions become bound with the opposite ions to form aggregated ions, hence the number of free ions decreases. The formation of contact ions leads to the decrease in the mobility of charge carriers, resulting in a decrease of the ionic conductivity of the electrolytes (see below). Furthermore, the fraction of “free” anions levels off at higher salt concentrations (O/Li<sup>+</sup> < 30). This may be attributed to the redissociation of “free” ions that occurred due to an increase in the system permittivity or dipole–dipole interactions.<sup>28</sup>

**DSC and TGA Studies.** DSC was used to examine the effects of LiClO<sub>4</sub> salt on the thermal transitions of these hybrids. Figure 3a shows the DSC curves obtained in the first scan for the salt-

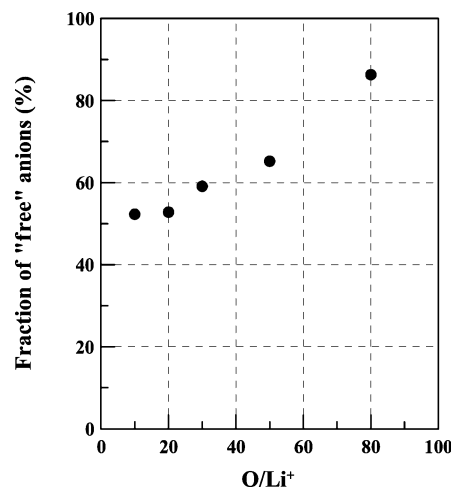
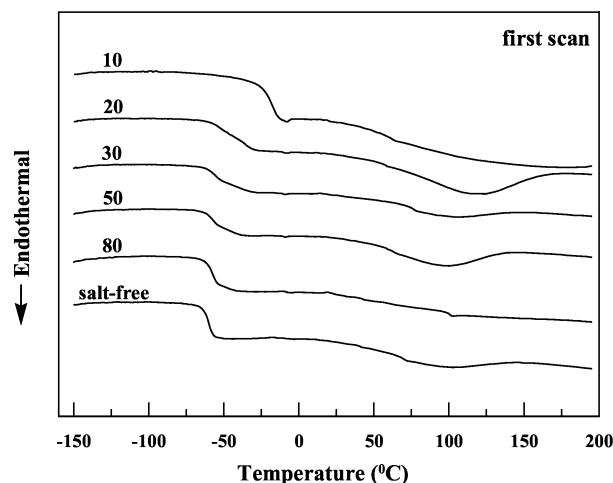


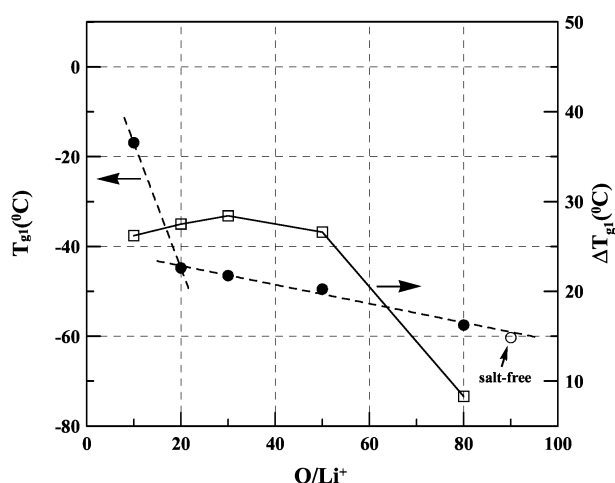
**Figure 2.** Fraction of spectroscopically “free” anions as a function of salt concentration for EDS–LiClO<sub>4</sub> system.

free EDS and EDS/LiClO<sub>4</sub> systems. As seen in Figure 3a, the undoped sample shows two second-order transitions at very different temperatures. These two transitions could be associated with the biphasic character of the polyether chains inside the hybrid networks. The polymer far away from silica networks behaves as an unrestricted polyether chain, possessing glass transition temperature,  $T_{g1}$ , at around −60.3 °C. On the contrary, the polymer near the silica nodes is more rigid due to the covalent bond with silica, showing transition at around 69 °C,  $T_{g2}$ . However, in our experimental conditions, no decoupling associated with different polyether segments (PEO and PPO) can be detected. Additionally, the relaxation peak at around 100 °C is observed. This may be attributed to the so-called physical aging effect due to the sample preparation conditions and thermal histories which the samples have experienced.<sup>29</sup>

Upon addition of LiClO<sub>4</sub> salt, as evidenced in Figure 3a, the thermal events change with increasing salt concentration. In comparison with the undoped sample, a significant change in  $T_{g1}$  with increasing LiClO<sub>4</sub> concentration is observed. Nevertheless, this behavior is less accentuated for the  $T_{g2}$ . Furthermore, at higher salt concentrations (O/Li<sup>+</sup> < 30), one high-temperature



(a)



(b)

**Figure 3.** (a) DSC curves obtained in the first scan for EDS–LiClO<sub>4</sub> electrolytes with various LiClO<sub>4</sub> concentrations (O/Li<sup>+</sup>); (b) variations in  $T_{g1}$  (●) and glass transition zone of  $T_{g1}$  (□) with salt concentrations for the undoped and LiClO<sub>4</sub>-doped EDS.

endothermic feature develops in the range of 115 to 180 °C, ascribing to the melting temperature of the crystalline phase of the polyether–LiClO<sub>4</sub> complex phase ( $T_{mc}$ ).<sup>30</sup> Table 1 and Figure 3b summarize the observed results of thermal measurements as a function of salt uptake. As seen in Figure 3b, the introduction of the salt in the polymer host leads to an increase in  $T_{g1}$  with increasing salt concentration, indicating a stiffening of the chain due to the ion–dipole interaction between the cation and the ether oxygens. Moreover, two regimes for the changes of  $T_{g1}$  with the salt concentration are obviously noticed. It can be proposed that in the low concentrated region, the LiClO<sub>4</sub> salt may interact preferentially with the oxirane-cleaved cross-link site of polymer host<sup>31,32</sup> and PEO block. At the highest salt concentration (O/Li<sup>+</sup> = 10), the cation complexation in the PPO block becomes more prominent, causing the raise of the rate of  $T_{g1}$  to increase. This can be further confirmed by <sup>7</sup>Li NMR measurements shown below.

Figure 3b also displays the value of the glass transition zone of  $T_{g1}$  ( $\Delta T_{g1}$ ) varied with the LiClO<sub>4</sub> uptake. This value reaches a maximum at the salt concentration of O/Li<sup>+</sup> = 30 and thereafter shows a slightly decreasing trend. The glass transition zone is defined as the difference between the onset and endset temperatures of the thermal transition process and reflects the

**TABLE 1: The DSC Results for EDS–LiClO<sub>4</sub> with Various Additions of Salt**

O/Li <sup>+</sup>	first scan				second scan		
	$T_{g1}$ (°C)	$\Delta T_{g1}$ (°C)	$T_{g2}$ (°C)	$T_{mc}$ (°C) <sup>a</sup>	$T_{g1}$ (°C)	$\Delta T_{g1}$ (°C)	$T_{g2}$ (°C)
∞	−60.3	6.1	69.0		−59.8	6.3	61.6
80	−57.3	8.3	99.3		−55.9	10.9	87.3
50	−49.5	26.6	61.9		−48.5	26.6	60.4
30	−46.5	28.4	75.3		−46.4	29.1	66.4
20	−44.8	27.5	56.3	118.8	−40.2	34.8	57.5
10	−16.9	26.2	61.4	174.1	−8.5	16.1	56.9

<sup>a</sup>  $T_{mc}$ : the melting point of crystalline PEO–LiClO<sub>4</sub> complex phase.

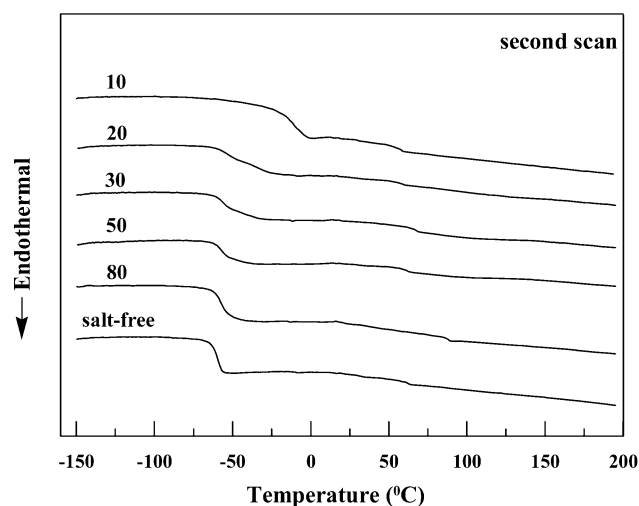
number of relaxation processes associated with the transition. Complexed polyether units may be located randomly along the polyether segments. The mutual influences on the behaviors of the free and complexed polyether units probably undergo relaxation processes with different relaxation times, resulting in the broadening of the glass transition. At a relatively high LiClO<sub>4</sub> concentration, almost all polyether units are complexed with LiClO<sub>4</sub>, and thus the distribution of the relaxation times becomes narrow again. Furthermore, the cations are expected to coordinate preferentially with the oxygens of the PEO block, because the solvating power of PEO is larger than that of PPO.

Interestingly, annealing the sample at 200 °C for 10 min to remove the thermal history makes the microstructure initially observed by DSC (in the first scan) less complex, as shown in Figure 4a. Apparently, the enthalpy relaxation peak as a result of the physical aging and the endothermic peak due to the melting of the crystalline polyether–LiClO<sub>4</sub> complex disappear, and the  $T_{g2}$  becomes evident. The absence of the physical aging and the melting peak for the crystalline complex phase in the second scan is probably due to the slow aging and recrystallization of the complex phase that cannot be completed during the short cooling interval between the first and the second scan. The process of heat treatment will involve the reorientation of the polymer matrix that would result in a microphase separation between polyether and siloxane segments; this is the reason that the  $T_{g2}$  is more apparent in the second scan.

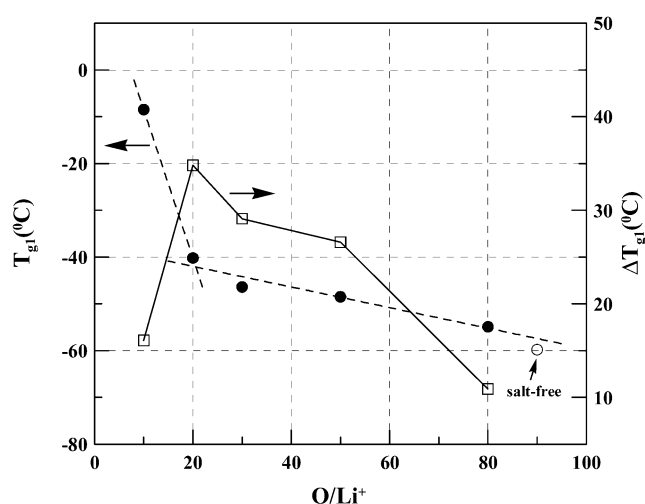
In addition, as seen in Table 1 for the samples doped with higher salt concentrations (O/Li<sup>+</sup> < 30), the observed  $T_{g1}$  values in the second scan are considerably higher than that in the first scan. One possible explanation is that the crystalline polyether–LiClO<sub>4</sub> complex has been destroyed during the heat treatment, and an increasing number of ether oxygens that can be coordinated to the Li<sup>+</sup> ions make the polyether segment more stiff and therefore raise the  $T_{g1}$  in the second scan. This behavior is also responsible for a maximum of the  $\Delta T_{g1}$  value at the salt concentration of O/Li<sup>+</sup> = 30 in the first scan shifting to that at O/Li<sup>+</sup> = 20 in the second scan, and an obviously decreasing trend thereafter, as shown in Figure 4b.

Thermogravimetric analysis (TGA) is used to measure the thermal stability of hybrid electrolytes. Figure 5 shows the weight loss behaviors of the salt-free EDS and EDS–LiClO<sub>4</sub> electrolytes investigated by TGA scanning from 100 to 800 °C under nitrogen. As shown in Figure 5, the undoped hybrid decomposes in a single step and the initial 10% weight loss ( $T_d^{0.1}$ ) occurs at around 360 °C. With further addition of salt, the creation of a second stage reflects the salt/polymer complex degradation, and the degradation rate of weight loss tends to increase with increasing LiClO<sub>4</sub> salt concentration. This behavior may be explained by the weakness of the C–O bond, caused by the decreased electronic density due to the O–Li<sup>+</sup> interaction. Alternatively, perchlorate oxidation of the polyether phase can cause this thermal event at ~500 °C.





(a)



(b)

**Figure 4.** (a) DSC curves obtained in the second scan for EDS–LiClO<sub>4</sub> electrolytes with various LiClO<sub>4</sub> concentrations (O/Li<sup>+</sup>); (b) variations in  $T_{g1}$  (●) and glass transition zone of  $T_{g1}$  (□) with salt concentrations for the undoped and LiClO<sub>4</sub>-doped EDS.

**<sup>13</sup>C CP/MAS NMR Spectra.** <sup>13</sup>C CP/MAS NMR spectra were carried out at different LiClO<sub>4</sub> concentrations to analyze the effect of the salt uptake on the polymeric chain and to study the chemical process involved. Figure 6 shows the <sup>13</sup>C CP/MAS NMR spectra of the polyether–siloxane hybrids doped with various amounts of LiClO<sub>4</sub>. As evidenced in this figure for the salt-free sample, there are three major peaks at ca. 70 ppm, which are associated with the polyether backbone moieties. Two peaks at 76 and 74 ppm are attributed to the PPO segments of D2000, whereas the peak at 71 ppm is assigned to the ether carbons in PEGDE.<sup>33</sup> The peak at 18 ppm is due to the methyl groups on the PPO backbone. Two peaks at 10 and 24 ppm are assigned to the methylene carbons in the α and β positions to the silicon atom, respectively. In addition, the peak at 57 ppm corresponds to those carbons adjacent to the nitrogen atom. Upon addition of LiClO<sub>4</sub> salt, it is obvious that the line broadening and the displacement to lower ppm values are observed with the peak of the methylene carbons in the PEO block (see the inset for comparison). These results indicate that the presence of lithium salts causes a more broad distribution of the PEO–segment environments and/or reduces the segmental

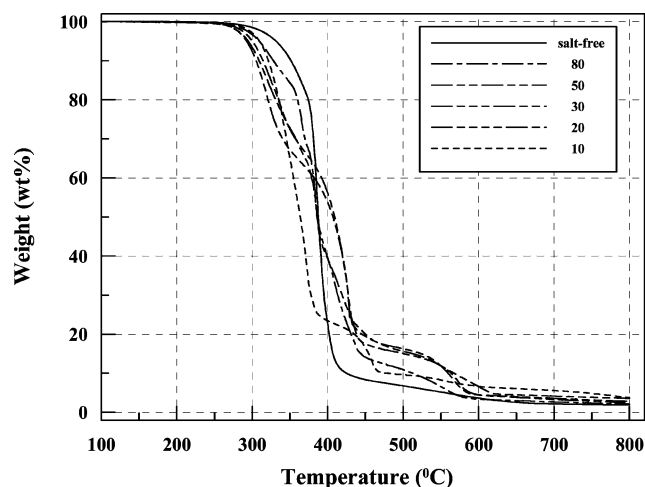


**Figure 5.** TGA thermograms of EDS–LiClO<sub>4</sub> complexes with various LiClO<sub>4</sub> concentrations (O/Li<sup>+</sup>) under nitrogen atmosphere.

motion of the polymer chains; the latter results from the electronic interaction between the Li<sup>+</sup> cations and the ether oxygens in PEO segments. However, this interaction is less pronounced for the peaks of methylene carbons adjacent to ether oxygens (76 and 74 ppm) and methyl groups (18 ppm) on the PPO segments until the salt concentration of O/Li<sup>+</sup> = 10. Such behavior coincides with the earlier DSC results that the abrupt raise of the rate of  $T_{g1}$  increases at the salt concentration of O/Li<sup>+</sup> = 10.

**<sup>7</sup>Li MAS NMR Spectra.** <sup>7</sup>Li MAS NMR measurement with high-power proton decoupling provides an extremely effective and unique method for probing different local environments of lithium cations in solid polymer electrolytes.<sup>34</sup> In this study, the proton-decoupled <sup>7</sup>Li MAS NMR spectra of EDS/LiClO<sub>4</sub> complexes as a function of salt concentration, recorded at 203 K, are displayed in Figure 7. As seen in Figure 7, for the sample doped with the salt concentration of O/Li<sup>+</sup> = 80, the line shape is asymmetric, and two well-resolved components at −0.2 (site I) and −0.9 ppm (site II) with integrated intensities of approximately 0.80:0.20 are observed, indicating that at least two distinct lithium species with different local environments exist in the polymer host, and the Li<sup>+</sup> cation is preferentially coordinated to site I. With further addition of LiClO<sub>4</sub> salt, obviously, the intensity of site II increases, where the intensity of site I is normalized, and a shoulder (site III) lying at ca. −1.4 ppm becomes visible at the highest salt concentrations of O/Li<sup>+</sup> = 10. Table 2 tabulates the variation of the relative intensities of the three components with different salt concentrations, as determined from the deconvolution of NMR spectra with the accuracy estimated at ±5%. On the basis of our previous study of epoxide-cross-linked polysiloxane/polyether electrolytes,<sup>32</sup> these three peaks are assigned to the lithium conformations as follows: the Li<sup>+</sup> cations coordinated with nitrogen atoms and/or polar hydroxyl groups in the polymer host (site I, −0.2 ppm) and with ether oxygens in polyether chains (site II, −0.9 ppm) and the formation of ion pairs or aggregates (site III, ca. −1.4 ppm), respectively. No direct evidence for lithium cation complexation in PEO and PPO chains can be observed in this study. Interestingly, as seen in Table 2 for the sample doped with the salt concentration of O/Li<sup>+</sup> = 10, the relative intensity of site II is significantly higher than that of site I, and also site III is visible at lower frequency. This result further supports the observations on the DSC curves which show a change for the rate of  $T_{g1}$  increase at the salt uptake of O/Li<sup>+</sup> = 20 as a result of the pronounced cation complexation in the PPO block.

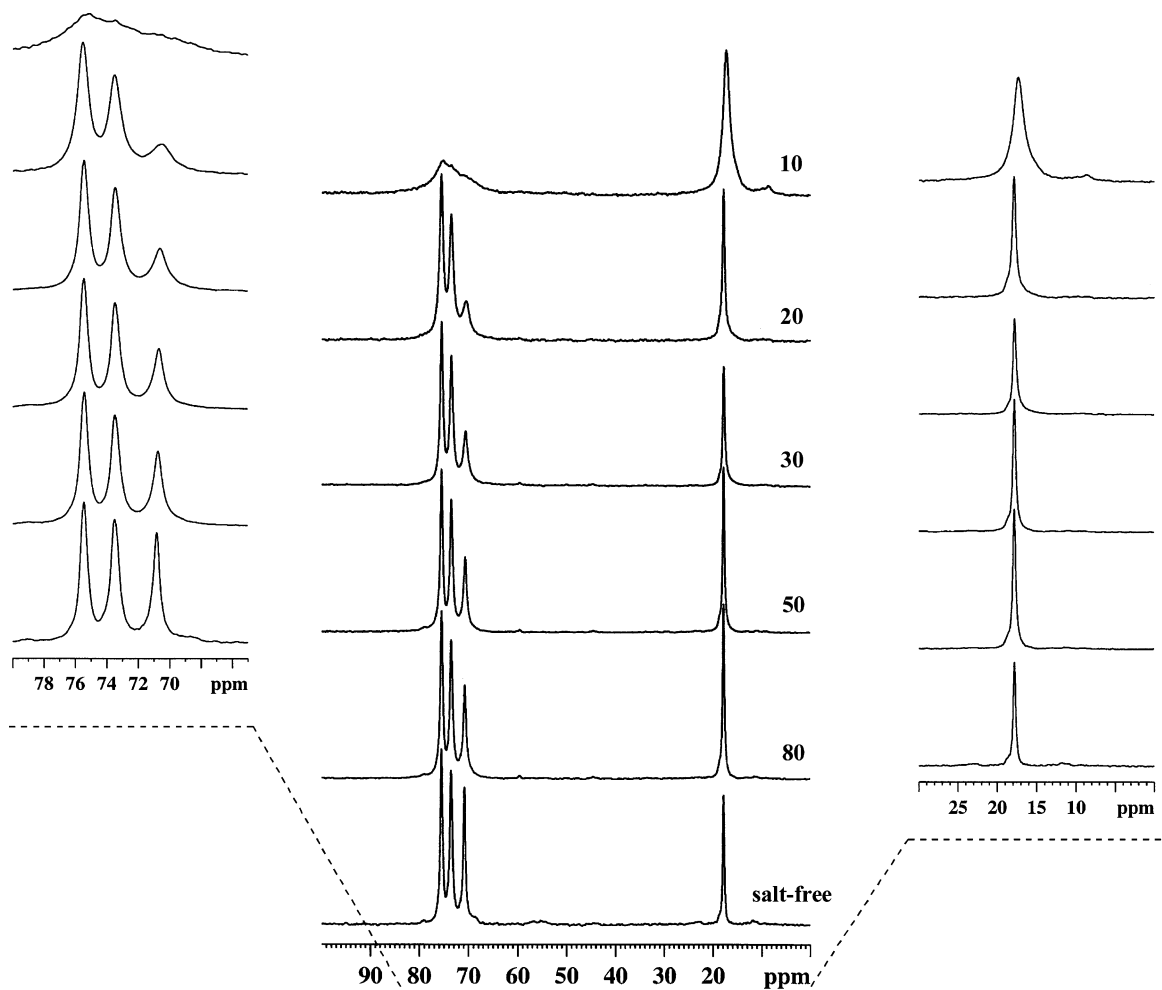


**Figure 6.**  $^{13}\text{C}$  CP/MAS spectra of EDS- $\text{LiClO}_4$  complexes doped with various salt concentrations ( $\text{O}/\text{Li}^+$ ). The ether carbon (ca. 70 ppm) and methyl carbon (18 ppm) regions are enlarged as shown in the inset.

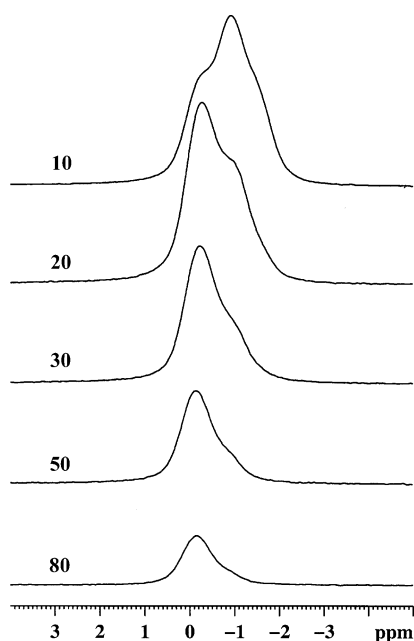


**Figure 7.**  $^7\text{Li}$  proton-decoupled MAS NMR spectra of EDS- $\text{LiClO}_4$  complexes with various salt concentrations ( $\text{O}/\text{Li}^+$ ), recorded at 203 K.

Additionally, the considerable formation of ion pairs or aggregates will result in a reduction in bulk ionic conductivity (see below).

**TABLE 2: The Deconvolution Results of Solid-State  $^7\text{Li}$  MAS NMR Spectra for EDS- $\text{LiClO}_4$  with Various  $\text{LiClO}_4$  Concentrations**

$[\text{O}]/[\text{Li}^+]$	peak area (%) <sup>a</sup>		
	site I	site II	site III
80	79.6	20.4	
50	73.8	26.2	
30	68.0	32.0	
20	60.5	39.5	
10	22.2	60.9	16.9

<sup>a</sup> The peak areas are based on the total integrated area.

**Ionic Conductivity Measurements.** As usually observed for ionic conductors, electrical impedance plotted in the complex plane exhibits an arc of the circle at higher frequencies that corresponds to the bulk conductivity of the samples, followed by an inclined linear variation at lower frequencies due to the interface between the sample and the blocking electrodes.<sup>35</sup> The intercept of the arc of the circle with the real axis gives the ohmic resistance from which conductivity can be deduced. With further addition of  $\text{LiClO}_4$  salt, in this study, the changes in free volume, electrostatic interactions, and hydrogen bonding certainly affect the ionic conductivity.

Figure 8a shows the temperature dependence of ionic conductivity ( $\sigma$ ) of the EDS/ $\text{LiClO}_4$  electrolyte films over a range of salt concentrations. As can be seen in this figure, the variation of conductivity with temperatures follows a VTF-like relationship,<sup>36–38</sup> which is indicative of ionic conductivity being coupled to polymer segmental motion. Figure 8b illustrates the

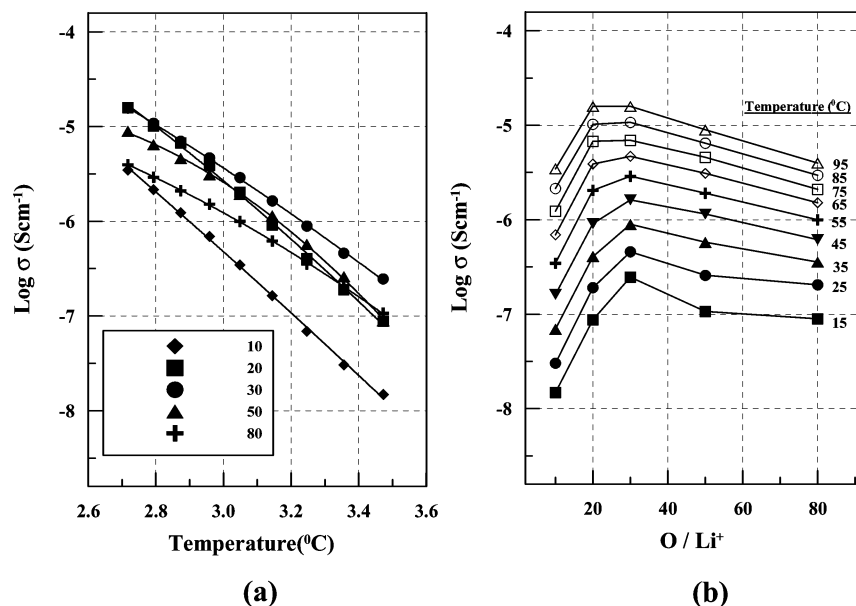


**Figure 8.** (a) Variation of ionic conductivity with temperature and (b) salt concentration dependence of ionic conductivity under various temperatures from 15 to 95 °C for the EDS–LiClO<sub>4</sub> complexes.

salt concentration dependence of ionic conductivity by examining isothermal plots. It is obvious that a maximum of conductivity can be observed in each analyzed temperature. From the conductivity data, it is clear that these ion transport behaviors cannot be explained by only the effect of the ionic mobility or of the number of carrier ions but are affected by the combination of these two effects. As seen in Figure 8b, the conductivity data pass through a maximum, suggesting that the effect of increasing the charge carrier density is overwhelmed by the accompanying decrease in segmental mobility and the increase in ionic association. The decrease in segmental mobility arising from transition cross-linking and the increase of ionic association leading to the formation of ion pairs or aggregates are verified by the earlier FT-IR, DSC, and <sup>13</sup>C and <sup>7</sup>Li NMR studies. At lower salt concentration levels ( $\text{O/Li}^+ > 30$ ), the extent of contact ion pairs is low, and consequently the conductivity is dominated by the number of charge carriers. At a relatively high LiClO<sub>4</sub> concentration, the formation of ion pairs or aggregates decreases the number density of charge carriers present, and also limits the mobility of the charge carriers throughout the polymer matrix; both effects result in a reduction in bulk ionic conductivity.

Furthermore, as seen in Figure 8b, the ionic conductivity maximum shifts to a higher salt uptake when the temperature is raised. As a result, the free volume theory is applied to discuss the ion transport mechanism. As the temperature increases, the amount of free volume increases, leading to the increase of ion and segment mobility, while the difference in the free volume of dissociated ions and polymer chains increases, resulting in a weakening of the cation–polymer interaction, which gradually favors the formation of ion pairs and ion aggregates.<sup>39,40</sup> At higher temperature, the negative effect on ionic conductivity at higher salt concentrations, resulting from the stiffening of polymer chains and the increase of ion association, can be counteracted by the positive effect on ionic conductivity, resulting from the increase of overall mobility of the electrolyte material.

## Conclusions

A series of the dual-cured polyether–siloxane hybrid electrolytes through epoxide cross-linking and inorganic polymer-

ization were prepared. The obtained chemical-covalent polyether–siloxane hybrid host consists of a fully amorphous phase and has a low glass transition temperature. The effect of the LiClO<sub>4</sub> salt-doped level on the microstructure and ionic conductivity in the hybrid host has been investigated. It is proposed that there is a change in cation complexation regime from the oxirane-cleaved cross-link site and PEO-block environments at lower salt-doped levels toward the PPO-block complexation, even with the formation of ion clusters at higher salt concentrations. The conductivity behavior follows VTF-like temperature dependence, suggesting that the charge-carrier transport is coupled with the segmental motion of the polymer host. These combined experiments show that a strong correlation between ion transport and ionic species exists in these hybrid electrolytes.

**Acknowledgment.** The authors would like to thank the National Science Council, Taipei, R.O.C. for their generous financial support of this research. The authors highly appreciated Ms. Ru-Rong Wu for her profound contribution in NMR experiments.

## References and Notes

- Gauthier, M.; Fauteux, D.; Vassort, G.; Belanger, A.; Duval, M.; Ricoux, P.; Chabagno, J. M.; Muller, D.; Rigaud, P.; Armand, M. B.; Deroo, D. *J. Electrochem. Soc.* **1985**, *132*, 1333.
- Scrosati, B. *Nature (London)* **1995**, *373*, 557.
- Gray, F. M. *Polymer Electrolytes, Fundamentals and Technological Applications*; The Royal Society of Chemistry: Cambridge, UK, 1997.
- Gray, F. M. *Solid Polymer Electrolytes*; VCH: Cambridge, UK, 1991.
- Acosta, J. L.; Morales, E. *J. Appl. Polym. Sci.* **1996**, *60*, 1185.
- Bruce, P. G. *Solid State Electrochemistry*; Cambridge University Press: Cambridge, UK, 1997; p 106.
- Berthier, C.; Gorecki, W.; Minier, M.; Armand, M. B.; Chabagno, J. M.; Rigaud, P. *Solid State Ionics* **1983**, *11*, 91.
- Fauteux, D.; Prud'Homme, J.; Harvey, P. E. *Solid State Ionics* **1988**, *28–30*, 923.
- Albinsson, I.; Mellander, B. E.; Stevens, J. R. *J. Chem. Phys.* **1992**, *96*, 681.
- Wu, P. W.; Holm, S. R.; Duong, A. T.; Dunn, B.; Kaner, R. B. *Chem. Mater.* **1997**, *9*, 1004.
- Wieczorek, W.; Raducha, D.; Zalewska, A.; Stevens, J. R. *J. Phys. Chem. B* **1998**, *102*, 8725.
- Croce, F.; Appetecchi, G. B.; Persi, L.; Scrosati, B. *Nature* **1998**, *394*, 456.

- (13) Popall, M.; Andrei, M.; Kappel, J.; Kron, J.; Olma, K.; Olsowski, B. *Electrochim. Acta* **1998**, *43*, 1155.
- (14) Münchow, V.; Noto, V. D.; Tondello, E. *Electrochim. Acta* **2000**, *45*, 1211.
- (15) Popall, M.; Durand, H. *Electrochim. Acta* **1992**, *37*, 1593.
- (16) de Zea Bermudez, V.; Alcacer, L.; Acosta, J. L.; Morales, E. *Solid State Ionics* **1999**, *116*, 197.
- (17) de Souza, P. H.; Bianchi, R. F.; Dahmouche, K.; Judeinstein, P.; Faria, R. M.; Bonagamba, T. J. *Chem. Mater.* **2001**, *13*, 3685.
- (18) Ravaine, D.; Seminel, A.; Charbouillot, Y.; Vincens, M. *J. Non-Cryst. Solids* **1986**, *82*, 210.
- (19) Brik, M. E.; Titman, J. J.; Bayle, J. P.; Judeinstein, P. *J. Polym. Sci. Part B: Polym. Phys.* **1996**, *34*, 2533.
- (20) Bermudez, V. Z.; Poinsignon, C.; Armand, M. *J. Mater. Chem.* **1997**, *7*, 1677.
- (21) Judeinstein, P.; Livage, J.; Zarudiansky, A.; Rose, R. *Solid State Ionics* **1988**, *28–30*, 1722.
- (22) Liang, W. J.; Chen, Y. P.; Wu, C. P.; Kuo, P. L. *J. Appl. Polym. Sci.* In press.
- (23) Salomon, M.; Xu, M.; Eyring, E. M.; Petrucci, S. *J. Phys. Chem.* **1994**, *98*, 8234.
- (24) Symons, M. C. R. *Electron–Solvent and Ion–Solvent Interactions*; Elsevier: New York, 1976; pp 311–341.
- (25) Kecki, Z. *Spectrochim. Acta* **1962**, *18*, 1155.
- (26) Kecki, Z. *Spectrochim. Acta* **1962**, *18*, 1165.
- (27) Salomon, M.; Xu, M.; Eyring, E. M.; Petrucci, S. *J. Phys. Chem.* **1994**, *98*, 8234.
- (28) Petrucci, S.; Eyring, E. M. *J. Phys. Chem.* **1991**, *95*, 1731 and the references therein.
- (29) Dusek, K. *Epoxy Resins and Composites IV*; Springer-Verlag: New York, 1986; p 126.
- (30) Lin, C. L.; Kuo, P. L.; Wu, R. R.; Kao, H. M. *Macromolecules* **2002**, *35*, 3083.
- (31) Ferry, A.; Oradd, G.; Jacobsson, P. *J. Chem. Phys.* **1998**, *108*, 7426.
- (32) Liang, W. J.; Kuo, P. L. *Macromolecules* **2004**, *37*, 840.
- (33) Liang, W. J.; Kao, H. M.; Kuo, P. L. *Macromol. Chem. Phys.* **2004**, *205*, 600.
- (34) Wang, H. L.; Kao, H. M.; Wen, T. C. *Macromolecules* **2000**, *33*, 6910.
- (35) Linford, R. G. *Electrochemical Science and Technology of Polymers*; Linford, R. G., Ed.; Elsevier Science: London, UK, 1990; Vol. 2, p 281.
- (36) Ratner, M. A. *Polymer Electrolyte Reviews I*; MacCallum, J. R., Vincent, C. A., Eds.; Elsevier: London, UK, 1987; p 173.
- (37) Lonergan, M. C.; Shriver, D. F.; Ratner, M. A. *Electrochim. Acta* **1998**, *40*, 204.
- (38) Mao, G.; Fernandez-Perea, R.; Howells, W. S.; Price, D. L.; Saboungi, M. L. *Nature* **2000**, *405*, 163.
- (39) Schantz, S.; Torell, L. M.; Stevens, J. R. *J. Chem. Phys.* **1991**, *94*, 6862.
- (40) Torell, L. M.; Jacobsson, P.; Petersen, G. *Polym. Adv. Technol.* **1993**, *4*, 152.